Nano Energy 41 (2017) 519–526

Contents lists available at ScienceDirect

Nano Energy

journal homepage: www.elsevier.com/locate/nanoen

Full paper

High-performance Si/organic hybrid solar cells using a novel cone-shaped Si nanoholes structures and back surface passivation layer

Zilei Wang[a], Shanglong Peng[a], Yuxiang Wen[a], Tianfeng Qin[a], Qiming Liu[a], Deyan He[a], Guozhong Cao[b,*]

[a] Key Laboratory for Magnetism and Magnetic Materials of the Ministry of Education, School of Physical Science and Technology, Lanzhou University, Lanzhou 730000, PR China

[b] Department of Materials Science and Engineering, University of Washington, Seattle, WA 98195-2120, United States

ARTICLE INFO

Keywords:
Hybrid solar cell
Surface nanotexturing
Light trapping
Surface charge recombination

ABSTRACT

Nanostructured silicon (Si) can provide improved light trapping capacity in Si/organic hybrid solar cells (HSCs) due to its low light reflectance compared with planar Si. However, the poor contact of nanostructured Si/organic interface and serious recombination on the uncovered Si surface can result in an inferior open-circuit voltage (V_{OC}) and fill factor (*FF*) for HSCs. Here, we have designed and fabricated a novel cone-shaped Si nanoholes (SiNHs) structures to form a superior interface contact between SiNHs and organic layer by using an advanced metal assisted chemical etching method. In addition, a Cs_2CO_3 layer was also introduced on the Si back surface to reduce the contact resistance as well as to suppress the surface recombination for the HSCs. With such improvements, a power conversion efficiency (PCE) up to 13.5% was achieved for Si/organic hybrid solar cell with the back passivation layer. This work provided a new strategy to improve the junction quality and performance of nanostructured Si/PEDOT:PSS HSCs.

1. Introduction

Recently, environment-friendly renewable energy has been widely investigated because of concerns with global warming and depletion of fossil fuels. Solar energy is one of the most abundant renewable energies and solar photovoltaic (PV) power generation is one of most scientific and sensible ways to utilize solar energy [1,2]. Crystalline silicon (Si) solar cell has played an important role in PV market due to its excellent optical properties, long-term stability and high power conversion efficiency (PCE). However, the severe demands of high vacuum and high temperature lead to a high cost of commercial Si-based solar cells and thus limit their use [3,4]. In order to reduce the cost, Si/organic hybrid solar cells (HSCs) have been developed in the past decade because they take advantage of the low cost processing for the organic materials [5]. Meanwhile, they have superior electrical properties such as high charge carrier mobility of the Si [6–11]. And the conducting polymer of poly (3,4-ethylenedioxythiophene):-polystyrene (PEDOT:PSS) is a suitable organic material to act as hole transporting and optical window as well as antireflection layer for the HSCs. It also serves as passivation layer [12]. When the spin-coated PEDOT:PSS thin films is used for HSCs, it can achieve noticeable performance including high open-circuit voltage (V_{OC}), short-circuit current density (J_{SC}) and fill factor (*FF*) [13,14].

Over past years, various methods have been utilized for improving the performance of HSCs, such as the modification of PEDOT:PSS layer [15,16], the addition of passivation layer at the interface [17,18]. However, the high reflectivity of planar Si limits the devices performance. Construction of different silicon nanostructures such as silicon nanowire arrays [12,19–22], silicon nanocones [23–26], hierarchical structure [27–29], was applied to allow more light absorption. An enhanced J_{SC} is usually obtained for the nanostructured Si-based solar cell [30,31]. Unfortunately, the quality of nanostructured PEDOT:PSS/Si SINH is poor, resulting in a serious electron-hole recombination and thus a low V_{OC}. Also, the PEDOT:PSS film is hard to penetrate into the gaps of the Si nanostructures due to the large surface tension of PEDOT:PSS, resulting in poor contact between Si and organics [22]. Consequently, it is extremely important to explore the optimal surface morphology including Si nanostructures density, multiscale texture and novel Si structures [21,27]. A strategy is to insert a layer of small molecules between textured Si and PEDOT:PSS layer to partially passivate the uncovered Si [32,33]. Sun et al. have developed a series methods for the modification of the Si nanostructures, including the density reduction of Si nanowires via using restructured Si with tetramethylammonium hydroxide (TMAH) [21], the contact improvement between Si and PEDOT:PSS layer by adding 3-glycidoxypropyltrimethoxydsilane (GOPS) [34]. He et al. have reported a

* Corresponding author.
E-mail addresses: pengshl@lzu.edu.cn (S. Peng), gzcao@u.washington.edu (G. Cao).

http://dx.doi.org/10.1016/j.nanoen.2017.10.011
Received 3 August 2017; Received in revised form 11 September 2017; Accepted 3 October 2017
Available online 03 October 2017
2211-2855/ Published by Elsevier Ltd.

cell that the PCE was improved to 16.2%, because the junction quality was promoted by a conformal diethyl phthalate (DEP) coating [35]. Traditionally, the Si-metal ohmic contact is synthesized by high doping at high temperatures (up to 1000 °C) to form the back surface field. This process requires the use of hazardous doping gases and poses operational and environmental issues. Additionally, a Schottky barrier at the metal/Si interface will be formed when the metal electrode was contacted with moderately doped-Si directly. The cesium carbonate (Cs_2CO_3) is an effective electron selective contact layer or hole-blocking layer at the cathode interface in hybrid solar cell to suppress the recombination of back surface [36]. From the above analysis, we reap a harvest that new strategies and insights are needed to improve the junction quality and performance of nanostructured Si/PEDOT:PSS HSCs.

In this paper, a simple method has been developed to adjust the diameter and density of irregular cone-shaped Si nanoholes (SiNH) with large opening area and shallow depth by using metal assisted chemical etching (MACE) method. In addition, a back passivation layer of Cs_2CO_3 was introduced to suppress the recombination of back surface. Through these structural improvements such as increasing the junction area and the light trapping capacity and reducing the recombination, a PCE of 13.5% was obtained with a J_{SC} of about 33 mA cm^{-2}, demonstrating a 43% increase compared with the planar Si HSCs.

2. Experimental section

One-side polished n-type Si (100) wafers (phosphorus-doped, 0.05–0.1 Ω cm) with a thickness of 300 μm were cut into 10 mm × 10 mm pieces. Then it was ultrasonically cleaned in acetone, ethyl alcohol, and deionized water for 20 min, respectively. Finally, the wafers were immersed in a diluted 5% HF solution for 3 min to remove the native oxide, receiving H termination and then washed with deionized water and dried.

Nanostructured Si was prepared via using a MACE process. First, Ag nanoparticles were deposited on Si wafers by immersing Si in a mixed solution of 5 M HF and 0.0 1 M $AgNO_3$, and then it was transferred into HF/H_2O_2 solution for 30 min at room temperature. The etched wafers were dipped into nitric acid for 20 min to remove Ag nanoparticles, and then rinsed with deionized water followed by dipping into 5% HF solution for 3 min, and the whole process was repeated 4 times. Finally, the samples were dried by a steam of N_2. We have also investigated the affection of deposition time and concentration of H_2O_2 on the morphology of nanostructured Si.

A conductive PEDOT:PSS (Clevios PH1000) solution mixed with the ethylene glycol (7 wt%) and Zonyl (0.1 wt%) was then spin-coated at a spin rate of 3000 rpm on the Si plat structure and 6000 rpm on the SiNHs structure for 40 s. Then the samples were annealed on a hot plate at 140 °C for 20 min to remove the solvents and formed the highly conductive p-type organic thin film. Then the Cs_2CO_3 and polyethylenimine (PEI) were dissolved in 2-methoxyethanol with concentrations of 0.5 mg mL^{-1} and 1 mg mL^{-1}, respectively, and a solution mixture of Cs_2CO_3/PEI (v/v = 1:1) used for the electron selective layer was spin coated onto the rear of Si structures. Finally, the Ag electrode was thermally evaporated on the top of the PEDOT:PSS layer, and a 300 nm-thick Al film was thermally evaporated onto the rear Si as back contact.

3. Results and discussion

Fig. 1 presents the schematics of c-Si/PEDOT:PSS HSCs with different configurations of front surface texturing and back passivation layer. The conventional nanostructured (conventional-SiNHs) SHCs is shown in the Fig. 1(a), The SiNHs are not covered with the PEDOT:PSS completely, which is due to the high density and small diameters of these holes , result in the PEDOT:PSS can't be penetrated in gaps. Thus it can introduce a large number of recombination centers in the SiNHs. Meanwhile, the small contact area between the PEDOT:PSS and Si implies few paths for photo-generated carriers separation and transportation, which indicates that the electrons and holes have a high probability to recombine at the interface, resulting in the deterioration of the cells photovoltaic performance including V_{OC}, J_{SC} and *FF*. In order to reduce the surface recombination, cone-shaped SiNHs with larger sizes can be fabricated via changing the H_2O_2 concentration from 0.4 to 4 M, which enable PEDOT:PSS to penetrate into SiNHs and form a conformal cladding as shown in Fig. 1(b). Similarly, the back surface of c-Si also has a high density of surface traps, which results in a high surface recombination, a large reverse saturation current, and a deteriorated ideal factor of the Si/PEDOT:PSS junction. Also, it can lead to an increase in contact resistance and thus a decrease in both *FF* and V_{OC}. In this paper, we introduce a Cs_2CO_3 passivation layer between the Si and the back-side metal electrode to solve these issues as shown in Fig. 1(c).

For the conventional MACE process, the Ag particles were first deposited on the Si surface, and the etching process was initiated once the sample was transferred into the etchant solution of 5 M HF and 0.4 M H_2O_2. On the contrary, in our study, a novel MACE process with 4 M H_2O_2 was used to avoid the formation of the SiNHs with small diameter and high density.

We have also investigated the effect of Ag deposition parameters and H_2O_2 concentration on the morphological characteristics of Si nanostructure. Firstly, the deposition time was explored with 15 s, 30 s, 45 s, 180 s, 10 min and 30 min. After deposition, the samples were transferred into etching solutions, containing 5 M HF and 4 M H_2O_2. The top view and cross section samples was measured by SEM as shown in Figs. S1–S4. We selected 45 s as the optimal deposition time, and Si was etched and formed the structure with diameters of about 300 nm, which is superior to that with other deposition times.

When samples deposited Ag was etched in an aqueous solution containing HF and H_2O_2, it can be found that cylindrical pores were generated in the direction perpendicular to the surface. Fig. 2. shows Si nanoholes structures with various concentration of H_2O_2. There is Si nanoholes with the size of 50 nm when the H_2O_2 concentration was

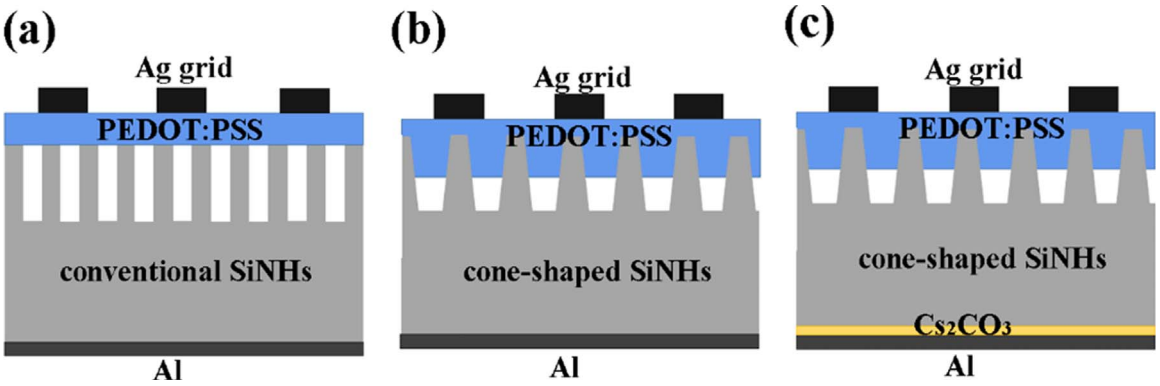

Fig. 1. Schematics of the device structures of c-Si/PEDOT:PSS HSCs with surface texturing by using metal assisted chemical etching method with different H_2O_2 concentrations. (a) Conventional SiNHs etching with 0.4 M H_2O_2, (b) cone-shaped SiNHs etching with 4 M H_2O_2 and (c) cone-shaped SiNHs etching with 4 M H_2O_2 combined with the back passivation layer of Cs_2CO_3.

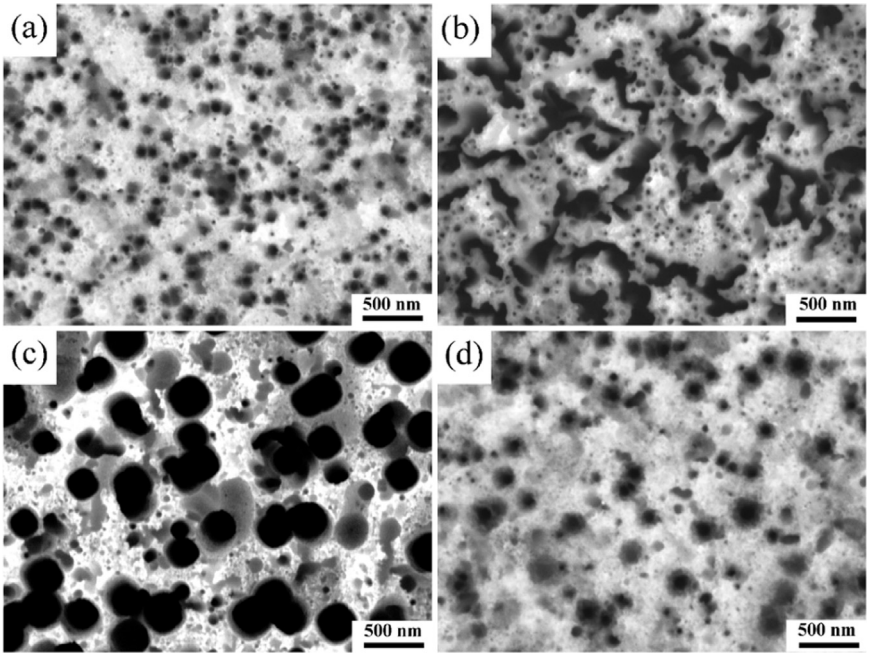

Fig. 2. Si nanostructures etching with HF/H_2O_2 solution by different concentration of (a) 0.4 M, (b) 2 M, (c) 4 M, and (d) 6 M.

0.4 M. The diameter of SiNHs was matched suitably with the Ag size as shown in Fig. S1(c). With increasing concentration of H_2O_2, the hole diameter became large and then the cone-shaped holes were formed. And the bottom diameter of the pore is identical to the Ag nanoparticle size, whereas the opening diameter of pore become large when 4 M H_2O_2 was used, as shown in Figs. 2(c) and 3(c). While a smooth surface at the macroscopic level was obtained when concentration was increased to 6 M. Si etching in presence of HF and H_2O_2 is based on localized microscopic electrochemical processes. The schema of these processes are shown in Fig. 4, and the reaction is as shown in Eq. (1):

$$Si + 6HF + \frac{n}{2}H_2O_2 \rightarrow H_2SiF_6 + nH_2O + \frac{4-n}{2}H_2 \quad (1)$$

where n is the number of holes per dissolved Si atom. This equation is written in a general form that accounts for the two dissolution regimes contained isotropous and anisotropic etching processes, as the

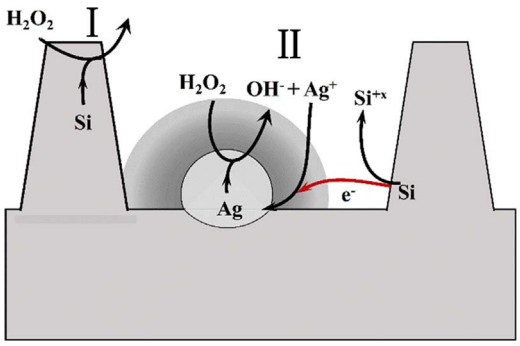

Fig. 4. Schematics of the potential reaction for the dissolution of silicon in the etch solution.

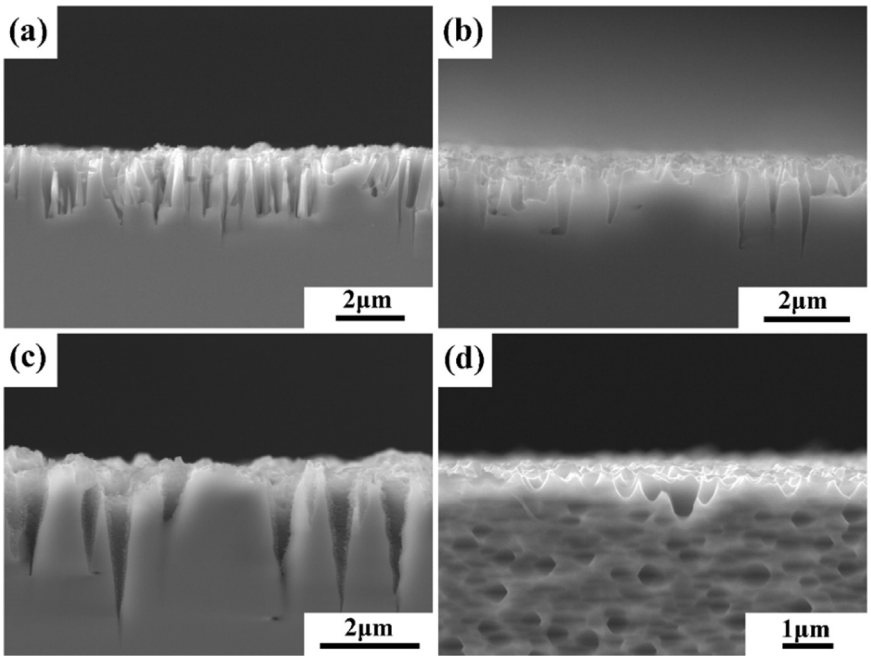

Fig. 3. The cross section of Si nanostructures etched by HF/H_2O_2 with the concentration of (a) 0.4 M, (b) 2 M, (c) 4 M, and (d) 6 M.

reactionIandIIshown in Fig. 4, respectively. This reaction is proceeding in a similar way of the chemical dissolution of Si in HF/HNO_3 [28–31]. When n = 2, H_2O_2 oxidizes the silver nanoparticles directly and form Ag^+, and in turn cycles back Ag^+ is reduced to Ag through the local oxidation of Si as shown in Fig. 4 of the reactionII, resulting in morphology of nanoholes. As show in Fig. 4, with the exception that H_2O_2 reacts with silver nanoparticles forming Ag+, reactionI that direct peroxide reaction on Si surface is occurred when the concentration of H_2O_2 was 6 M. Therefore, the bulk etching predominates decreasing the height of nanoholes and increasing nanowire taper as seen in Fig. 2(d).

In metal assisted chemical etching process, it is localized at the Si/metal nanoparticle interface due to the catalytic properties of the metal for the reduction of H_2O_2. From the reactionII, it is also clearly that holes are consumed with the similar size of Ag nanoparticle. It could be that surface reactions are faster than holes diffusion due to an effective coupling between the Si valence bonds and the Ag energy levels, or that a charge depletion layer exists around the Ag particles with a lower energy barrier for holes at the Ag/Si interface than that at the HF/Si interface [37–39]. In any case, the fact that local etching occurs in low concentrated H_2O_2 solutions indicates that the lack of oxides at the Ag/Si interface is an important parameter. As a consequence of local etching, well-separated cylindrical pores are formed with diameter closely matching those of the nanoparticles (Figs. S1(c) and 2(a)). The diameters were enlarged with the increasing the H_2O_2 concentration as shown in Fig. 2(b), it is ascribed to that oxides is sufficient, the particle penetration rate decreases. This indicates that more holes are consumed at the pore walls than that at the pore tips, it makes the pore widening instead of pore deepening. With the further increase of oxides concentration, cone-shaped pores with diameter larger than the Ag nanoparticle dimensions are indeed observed in Figs. 2(c) and 3(c). When the concentration of H_2O_2 is 2 M the pore diameter is around 100 nm and increases up to about 300 nm at the concentration of H_2O_2 of 4 M. A possible explanation is as the following. When the H_2O_2 concentration increases from 0.4 to 4 M, an oxide layer will be built at the Si/Ag interface, injected holes may diffuse away from the pore tip. Holes diffuse to the pore walls as a spread current which is lower than J_{PS} (the critical current density of metal-assisted chemical etching process), resulting in the formation of micro-porous Si on the walls. While in Fig. 2(d), the diameters of pores are suppressed severely, because of the surplus of oxides besides reactionII,and reactionIbegins reacting that cause a isotropous etching in Si surface. It is also observed in Fig. 3(d).

The cross section images of Si substructure with spin-coated PEDOT:PSS are shown in Fig. 5. As shown in Fig. 5(c), the PEDOT:PSS was penetrated in gaps of cone-shaped SiNHs, compared with the structure of Si nanoholes etched with 0.4 M H_2O_2 as shown in Fig. 5(b), which offers more advantageous contact and therefore a high *FF*, V_{OC} were obtained.

The current-voltage (J-V) curves of three types c-Si/PEDOT:PSS HSCs made from the planar Si, the conventional-SiNHs and the cone-shaped SiNHs under the illuminated and in the dark are illustrated in Fig. 6(a) and (b), respectively, and the main characteristic of photovoltaic combined with J_{SC}, V_{OC}, *FF*, PCE are listed in Table 1. The planar Si/PEDOT:PSS HSCs display an *FF* of 69.1% because of the favorable contact between Si and organic film, but high light reflectance caused by planar Si delivers an unsatisfactory current density. On the contrary, the device based on conventional SiNHs shows a higher J_{SC}, because an excellent light harvesting capacity will be achieved via the formation of these nanostructures with high density and small diameters after conventional MACE process. Unfortunately, it also leads to poor *FF* and V_{OC} due to the PEDOT:PSS film was floated on the Si surface, which results in an undesirable contact, and there is a mass of recombination center at uncovered Si surface. The device exhibits a PCE of 9.43%, which is even lower than that of planar junction solar cell. These issues were solved via the use of novel MACE process, as shown in Fig. 6(a) and (b), a satisfactory improvement of all parameters, especially *FF* and V_{OC}, are obtained. The enhanced photovoltaic performance can be mainly ascribed to the improvement of junction quality as shown Fig. 5. Compared with that of the conventional SiNHs counterpart, A J_{SC} of 32.5 mA cm^{-2}, V_{OC} of 618.1 mV, *FF* of 64.9% are obtained and thus a PCE of 13.04% is achieved, which presents nearly 6.9%, 14.1%, 14.5%, 38.3% enhancement of J_{SC}, V_{OC}, *FF*, and PCE, respectively. In addition, the *J-V* curves of four type structures cells etched by H_2O_2 with various concentration of 0.4 M, 2 M, 4 M, 6 M, are shown in Fig. S5, and the main parameters are listed in Table S1.

In addition, the J-V curves of these three types HSCs in dark condition is illustrated in Fig. 6(b). It can be found that the leakage current will lead to the decrease of V_{OC}, so the reverse saturation current density (J_0) must be reduced to attain a satisfactory V_{OC}. In theory, the dark J-V curves can be simulated using the Eq. (2):

$$J_{dark}(V) = J_0\left[exp\left(\frac{eV}{nkT}\right) - 1\right] \quad (2)$$

where n is the diode ideality factor, k is the Boltzmann constant, T is the temperature and *e* is charge of an electron. The J_0 and the diode ideality factor (*n*) can be determined using numerical fit to the *J-V* curves in dark condition by the least square fitting, and the value of both n and J_0 was shown in Table 2. From the Table, the *n* values of the conventional SiNHs HSC is 3.35, which higher than that of planar structure (2.86) and cone-shaped SiNHs structure (1.9), indicating the interface quality was improved by using the cone-shaped SiNHs structure [40].

These results are conformed to the PCE value and should be strongly associated with the density of interfacial states (DIS) between Si and organic. According to the Yu, the value of DIS should be proportional to the specific surface of Si nanostructures [41]. Thus it can be deduced that the cone-shaped SiNHs have introduced lower DIS than that of the conventional SiNHs, but higher than that of the Planar-Si. For the conventional SiNHs, the PEDOT:PSS interfaces contain interfacial states that cause Fermi-level pining, limit the V_{OC}, and poor contact and thus result in the small shunt resistance between Si and PEDOT:PSS film, leading to the decrease of FF for device. Since the cone-shaped SiNHs/PEDOT:PSS solar cell has much low DIS, the band bending near the

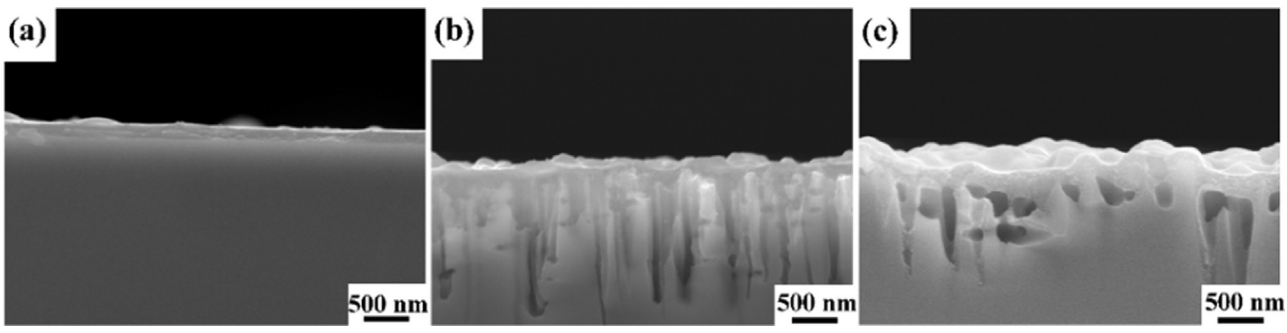

Fig. 5. The cross section of Si nanostructures after spin-coating PEDOT:PSS: (a) planar-Si, (b) conventional Si nanostructure using 0.4 M H_2O_2, (c) cone-shaped Si nanostructure using 4 M H_2O_2.

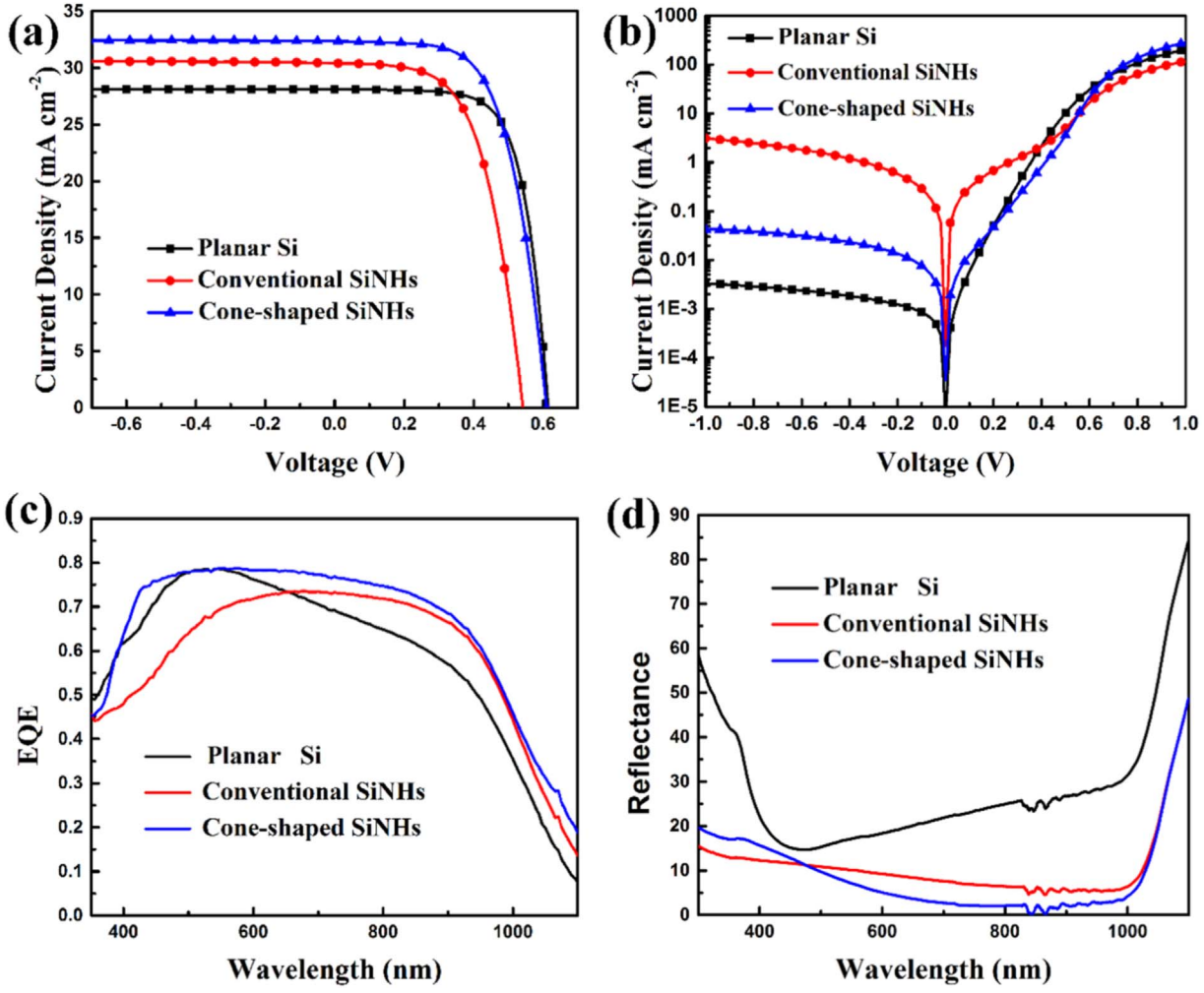

Fig. 6. Photovoltaic characterization of the HSCs with different Si structures (a) under the standard AM1.5 G condition, (b) in the dark condition, (c) external quantum efficiency (EQE) spectra of these devices, (d) reflectance curves of various Si structure after spin coating of PEDOT:PSS.

Table 1
Photovoltaic characteristics of HSCs with different structures.

Samples	J_{SC} (mA cm^{-2})	V_{OC} (mV)	*FF* (%)	PCE (%)
Planar Si	**28.1**	**618.3**	**69.1**	**11.98**
Conventional	**30.4**	**541.5**	**57.3**	**9.43**
Cone-shaped	**32.5**	**618.1**	**65.6**	**13.04**

Table 2
List of the ideality factor (n), and the reversed saturation current (J_0) obtained from dark J –V curves based different structures of HSCs.

Samples	J_0 (mA cm^{-2})	n
Planar Si	1.41×10^{-6}	1.9
Conventional	7.34×10^{-5}	3.35
Cone-shaped	1.09×10^{-5}	2.86

silicon surface is mainly dependent on the difference of Fermi levels between Si and PEDOT:PSS, instead of the interface states, which benefits the decrease of minority carrier (hole) recombination rate at Si/PEDOT:PSS interface, results in an increase of *V*oc. Meanwhile, for the cone-shaped nanoholes, the contact between Si and organic film still poor than that of planar one, so the FF value for cone-like nanoholes devices are worse than that of the planar device.

The value of V_{OC} is associated with built-in voltage (V_{bi}) positively. As shown in the Fig. 7(a), the V_{bi} could be deduced by $V_{bi} = (\Phi_{B0} - \Phi_n)/q$, in which Φ_{B0} is Schottky barrier height and the Φ_n is the energy difference between conduction band (E_C) edge and Fermi level (E_F) of the Si substrate. It can be deduced that the value of V_{bi} for the cone-shaped SiNHs HSCs should have an obvious improvement because of the suppressed of DIS. In a typical p-n junction, V_{OC} can also be described followed equation:

$$V_{OC} = \frac{kT}{q} \ln \left(\frac{J_{SC}}{J_0} + 1\right) \quad (3)$$

According to Eq. (3) and the value of J_0 in Table 2, it can be deduced that the V_{OC} for both planar-Si/PEDOT:PSS and cone-shaped SiNHs/PEDOT:PSS HSCs are larger than that for the conventional SiNHs/PEDOT:PSS one. Also, the capacitance-voltage (C^{-2}-V) curves were measured to examine the electronic performance of the devices with different structures as shown in Fig. 7(b). It can be found that the planar Si and cone-shaped SiNHs HSCs present a similar V_{bi} value about 694.2 mV and 686.3 mV, but a value of only 632.2 mV was obtained in conventional SiNHs HSCs, this result is conformed to the conclusion from the Fig. 7(a) and Eq. (3).

External quantum efficiency (EQE) spectra of the HSCs with different configurations are measured as shown in Fig. 6(c). The EQE is the percentage of the number of charge carriers collected at the electrode under short-circuit condition to the number of incident photos, and for the HSCs, this ratio value is dependent on four major steps. Thus, the EQE can be expressed as:

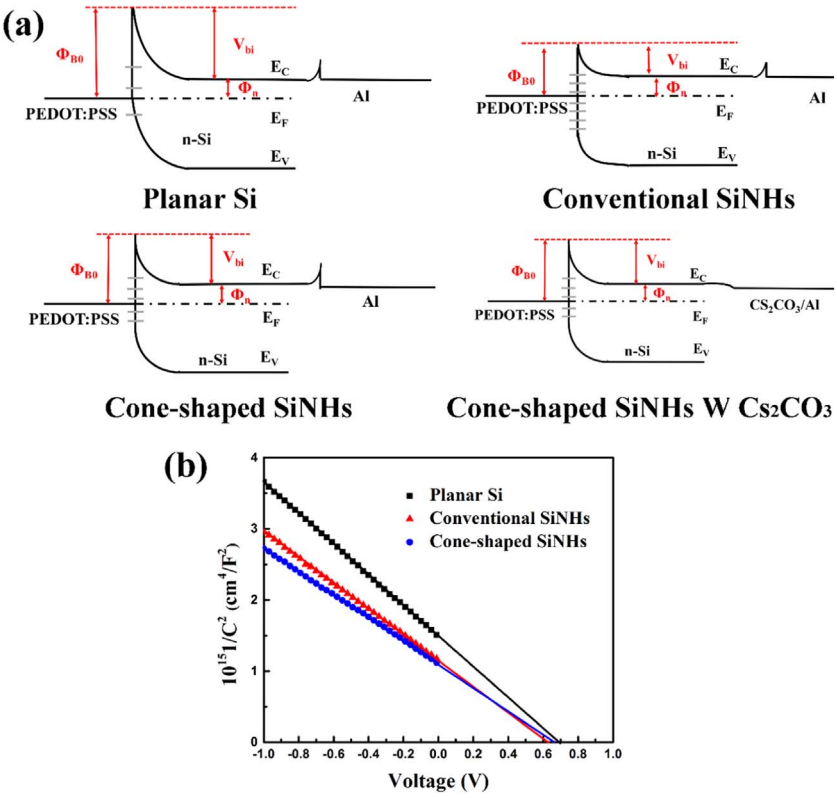

Fig. 7. (a) Band alignment at the Si/PEDOT:PSS interface with different structure, (b) C^{-2}-V plots of the Si/PEDOT:PSS devices with different structures.

$$EQE = \eta_{abs} \times \eta_{diff} \times \eta_{diss} \times \eta_{cc} \quad (4)$$

The scheme of this process is display in Fig. 8. The parameter η_{abs} describes the absorption yield of the device, and this represents the most effective way of increasing the J_{SC}. The η_{diff} and η_{diss} describe the efficiency of the photo-generated electrons and holes diffuse to Si/organic interface and dissociate at interface, this factor is inversely related to the rate of recombination within the material and interface, and related to the value of V_{bi}. The η_{cc} describes the efficiency of charge collection at the electrodes. The J_{SC} is directly related to the EQE, and this relationship can be expressed as:

$$J_{SC} = \frac{q}{\hbar c} \int_{\lambda_{min}}^{\lambda_{max}} EQE \times P_{in}(\lambda)\lambda \times d\lambda \quad (5)$$

From the Fig. 6(c), the devices with cone-shaped structure enhanced EQE values in the wavelength range from 350 to 1100 nm, especially in the visible and near-infrared regime, which is ascribed to the increase of η_{abs} by the light trapping structure. In the cone-shaped SiNHs cells, the interfacial recombination between Si and organic is restrained, and results in a promotion of η_{diff} and η_{cc}, thus the device displays an unexpected improvement in the wavelength range of 400–900 nm, approaching an EQE value about 80%. The EQE value of conventional SiNHs cell is terribly in the range of 350–600 nm, while a J_{SC} of 30.4 mA cm^{-2} is obtained which higher than that of planar Si cell,

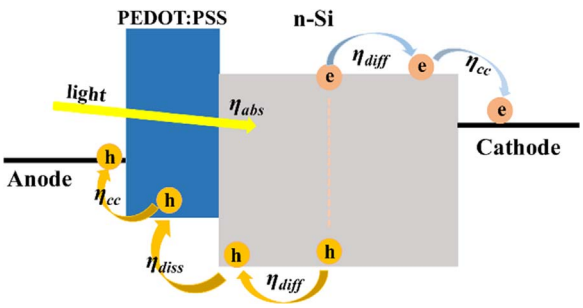

Fig. 8. The schematic of the process that carriers diffuse, dissociate, and collect.

which is due to that the long wavelength has higher photo flux density under the standard AM1.5 G condition compared with short wavelength range [42,43].

It is worth noting that the respective reflection values of those different devices are distinguishing distinctly, as illustrated in Fig. 6(d). The reflectance is decreased enormously in the whole range and show a value under 20% after etching because of the light trapping capacity of Si nanostructures. The value of cone-shaped structure is lower than that of the traditional SiNHs, which is due to that the absorption is increased by the enlarged diameter of nanoholes in long wavelength range. After spin coating, the PEDOT:PSS film was floated on conventional SiNHs surface, while after the formation of cone-shaped structure, the film was penetrated into these gaps and causes the surface roughly, and this is other reason why the reflectance was lower than that of the conventional SiNHs structure. Therefore, the enhanced EQE may be mainly ascribed to the suppression of light reflectance from planar Si to nanostructured Si, and the improvement of the junction quality from conventional SiNHs to cone-shaped structure, as discussed above.

Finally, we further introduced the Cs_2CO_3 passivation layer into the cone-shaped SiNHs HSCs. As shown in Fig. 7(a), there was a large barrier between Al and Si, and electron have to pass through this barrier to be collected by Al. For the Cs_2CO_3 contact layer, the barrier was dramatically reduced. In addition, charge recombination was also suppressed. The cone-shaped SiNHs/PEDOT:PSS HSCs with a Cs_2CO_3 passivation layer delivers a best performance contain J_{SC} of a 32.9 mA cm^{-2}, a V_{OC} of 627.9 mV, a *FF* of 65.8%, and yields a PCE of 13.5%. And the *J-V* curves under light and in the dark are shown in Fig. 9(a) and (b). The introduction of the back passivation layer reduces the recombination at the back surface and results in a promotion of η_{cc}, thus the HSSs with the back passivation layer present the improvement of EQE with a value of more than 80% in the visible and near-infrared regime. The device structure is shown in Fig. 9(d) which presents the optimal performance.

4. Conclusions

A novel structure of cone-shaped SiNHs has developed to improve

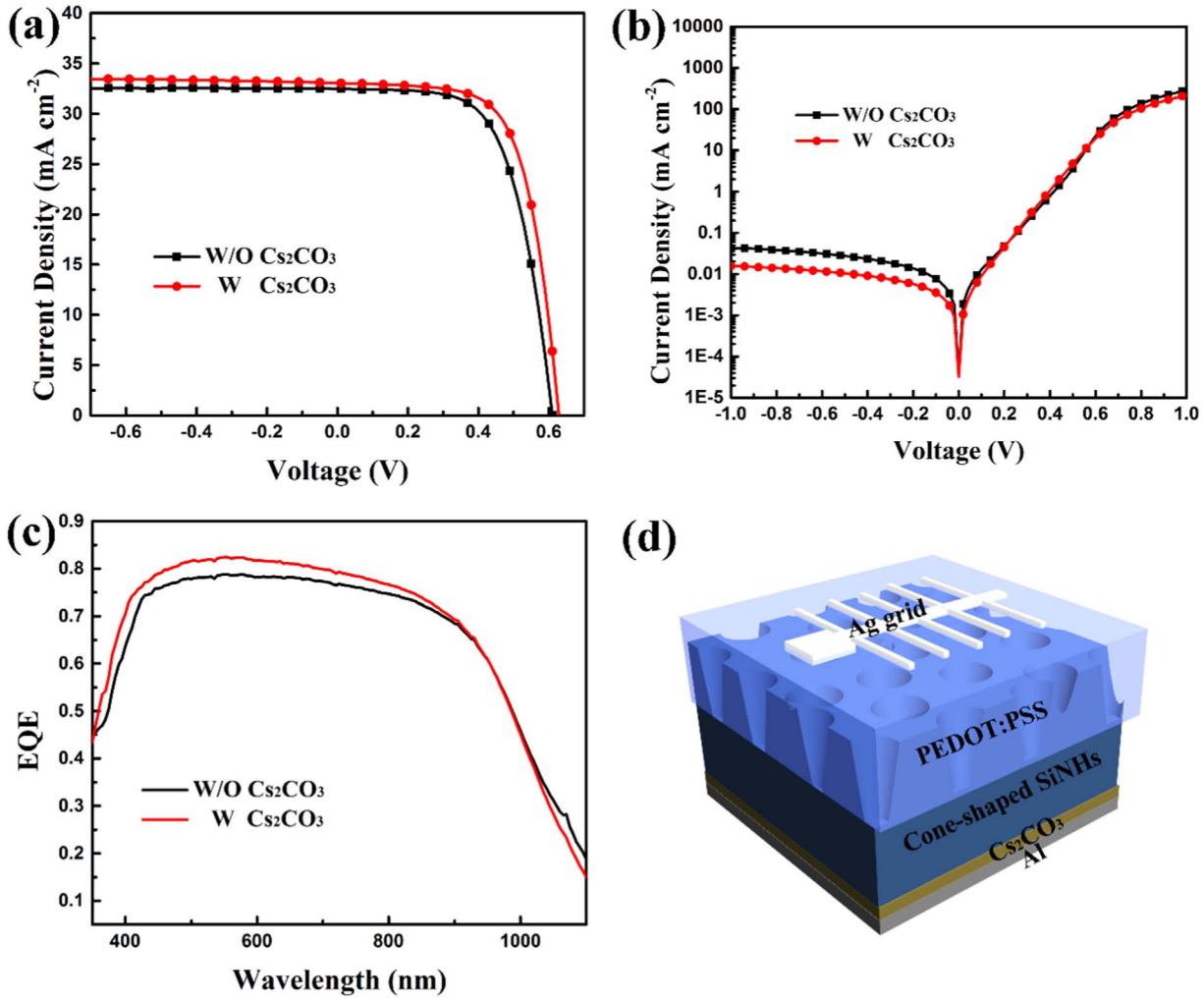

Fig. 9. Photovoltaic characterization of the cone-shaped SiNHs/PEDOT:PSS HSCs with and without back passivation layer (a) under the standard AM1.5 G condition, (b) in the dark condition, (c) external quantum efficiency (EQE) spectra of these devices, (d) the schematic of the device structure.

light trapping and to form an excellent contact between Si and PEDOT:PSS for HSCs. In addition, a Cs_2CO_3 layer was also introduced on the Si back surface to reduce the contact resistance as well as to suppress the surface recombination for the HSCs. Through these improvements, a PCE of 13.5% is achieved with an excellent current density of 32.9 mA cm^{-2} for HSCs based the cone-shaped SiNHs. The improved performance can be ascribed to the predominant optical property, improved heterojunction quality and the reduced recombination on both surface. This study also offers a design guideline for high performance Si nanostructures HSCs with a superior balancing in electrical and optical characteristics, which can potentially improve the performance of HSCs.

Acknowledgments

This work was financially supported by National Natural Science Foundation of China (Grant No. 61376011) and the Fundamental Research Funds for the Central Universities (No. lzujbky-2017-k21).

Appendix A. Supplementary material

Supplementary data associated with this article can be found in the online version at http://dx.doi.org/10.1016/j.nanoen.2017.10.011.

References

[1] X. Wang, D. Jing, M. Ni, Sci. Bull. 62 (9) (2017) 597–598.
[2] R. Perez, P. Ineichen, R. Seals, J. Michalsky, R. Stewart, Sol. Energy 44 (5) (1990) 271–289.
[3] P. Woditsch, W. Koch, Sol. Energy Mater. Sol. Cells 72 (1–4) (2002) 11–26.
[4] S. Pizzini, M. Acciarri, S. Binetti, Phys. Status Solidi (a) 202 (15) (2005) 2928–2942.
[5] M. Wang, Sci. Bull. 62 (4) (2017) 249–255.
[6] R. Liu, S.T. Lee, B. Sun, Adv. Mater. 26 (34) (2014) 6007–6012.
[7] M. Zhao, J. Zhang, N. Gao, P. Song, M. Bosman, B. Peng, B. Sun, C.W. Qiu, Q.H. Xu, Q. Bao, K.P. Loh, Adv. Mater. 28 (16) (2016) 3138–3144.
[8] C.-Y. Liu, Z.C. Holman, U.R. Kortshagen, Nano Lett. 9 (1) (2009) 449–452.
[9] Z.-Y. Li, Y.-Z. Wang, L.-M. He, H.-J. Zheng, Sci. Rep. 4 (3895) (2014) 1–7.
[10] Q. Liu, M. Ono, Z. Tang, R. Ishikawa, K. Ueno, H. Shirai, Appl. Phys. Lett. 100 (18) (2012) 183901.
[11] X. Mu, X. Yu, D. Xu, X. Shen, Z. Xia, H. He, H. Zhu, J. Xie, B. Sun, D. Yang, Nano Energy 16 (2015) 54–61.
[12] L. He, C. Jiang, H. Wang, D. Lai, Rusli, ACS Appl. Mater. Interfaces 4 (3) (2012) 1704–1708.
[13] Y.C. Lai, Y.F. Chang, P.T. Tsai, J.K. Chang, W.H. Tseng, Y.C. Lin, C.Y. Hsiao, H.W. Zan, C.I. Wu, G.C. Chi, H.F. Meng, P. Yu, Opt. Express 24 (2) (2016) A414–A423.
[14] M. Pietsch, S. Jäckle, S. Christiansen, Appl. Phys. A 115 (4) (2014) 1109–1113.
[15] S. Jackle, M. Liebhaber, J. Niederhausen, M. Buchele, R. Felix, R.G. Wilks, M. Bar, K. Lips, S. Christiansen, ACS Appl. Mater. Interfaces 8 (13) (2016) 8841–8848.
[16] X. Jiang, Z. Wang, W. Han, Q. Liu, S. Lu, Y. Wen, J. Hou, F. Huang, S. Peng, D. He, G. Cao, Appl. Surf. Sci. 407 (2017) 398–404.
[17] Y. Liu, Z.G. Zhang, Z. Xia, J. Zhang, Y. Liu, F. Liang, Y. Li, T. Song, X. Yu, S.T. Lee, B. Sun, ACS Nano 10 (1) (2016) 704–712.
[18] J.P. Thomas, K.T. Leung, Adv. Funct. Mater. 24 (31) (2014) 4978–4985.
[19] L. He, C. Jiang, H. Wang, D. Lai, Y. Heng Tan, C. Seng Tan, Rusli, Appl. Phys. Lett. 100 (10) (2012) 103104.
[20] W. Lu, C. Wang, W. Yue, L. Chen, Nanoscale 3 (9) (2011) 3631–3634.

[21] J. Zhang, T. Song, X. Shen, X. Yu, S.-T. Lee, B. Sun, ACS Nano 8 (11) (2014) 11369–11376.
[22] P. Yu, C.-Y. Tsai, J.-K. Chang, C.-C. Lai, P.-H. Chen, Y.-C. Lai, P.-T. Tsai, M.-C. Li, H.-T. Pan, Y.-Y. Huang, Chih-IWu, Y.-L. Chueh, S.-W. Chen, C.-H. Du, S.-F. Horng, H.-F. Meng, ACS Nano 7 (12) (2013) 10780–10787.
[23] S. Jeong, E.C. Garnett, S. Wang, Z. Yu, S. Fan, M.L. Brongersma, M.D. McGehee, Y. Cui, Nano Lett. 12 (6) (2012) 2971–2976.
[24] H. Wang, J. Wang, Rusli, Nanoscale Res. Lett. 10 (2015) 191.
[25] Z. Ying, M. Liao, X. Yang, C. Han, J. Li, J. Li, Y. Li, P. Gao, J. Ye, IEEE J. Photovolt. 6 (4) (2016) 888–893.
[26] P. Gao, H. Wang, Z. Sun, W. Han, J. Li, J. Ye, Appl. Phys. Lett. 103 (25) (2013) 253105.
[27] J. He, Z. Yang, P. Liu, S. Wu, P. Gao, M. Wang, S. Zhou, X. Li, H. Cao, J. Ye, Adv. Energy Mater. 6 (8) (2016).
[28] W.R. Wei, M.L. Tsai, S.T. Ho, S.H. Tai, C.R. Ho, S.H. Tsai, C.W. Liu, R.J. Chung, J.H. He, Nano Lett. 13 (8) (2013) 3658–3663.
[29] J. He, P. Gao, M. Liao, X. Yang, Z. Ying, S. Zhou, J. Ye, Y. Cui, ACS Nano 9 (6) (2015) 6522–6531.
[30] K. Sato, M. Dutta, N. Fukata, Nanoscale 6 (11) (2014) 6092–6101.
[31] X. Shen, B. Sun, D. Liu, S.-T. Lee, J. Am. Chem. Soc. 133 (48) (2011) 19408–19415.
[32] F. Zhang, D. Liu, Y. Zhang, H. Wei, T. Song, B. Sun, ACS Appl. Mater. Interfaces 5 (11) (2013) 4678–4684.
[33] Y.T. Lee, F.R. Lin, C.H. Chen, Z. Pei, ACS Appl. Mater. Interfaces 8 (50) (2016) 34537–34545.
[34] S. Wu, W. Cui, N. Aghdassi, T. Song, S. Duhm, S.-T. Lee, B. Sun, Adv. Funct. Mater. 26 (28) (2016) 5035–5041.
[35] J. He, P. Gao, Z. Yang, J. Yu, W. Yu, Y. Zhang, J. Sheng, J. Ye, J.C. Amine, Y. Cui, Adv. Mater. (2017).
[36] Y. Zhang, W. Cui, Y. Zhu, F. Zu, L. Liao, S.-T. Lee, B. Sun, Energy Environ. Sci. 8 (1) (2015) 297–302.
[37] K.Q. Peng, J.J. Hu, Y.J. Yan, Y. Wu, H. Fang, Y. Xu, S.T. Lee, J. Zhu, Adv. Funct. Mater. 16 (3) (2006) 387–394.
[38] K. Peng, H. Fang, J. Hu, Y. Wu, J. Zhu, Y. Yan, S. Lee, Chemistry 12 (30) (2006) 7942–7947.
[39] C. Chartier, S. Bastide, C. Lévy-Clément, Electrochim. Acta 53 (17) (2008) 5509–5516.
[40] X. Zhang, D. Yang, Z. Yang, X. Guo, B. Liu, X. Ren, S.F. Liu, Sci. Rep. 6 (2016) 35091.
[41] X. Yu, X. Shen, X. Mu, J. Zhang, B. Sun, L. Zeng, L. Yang, Y. Wu, H. He, D. Yang, Sci. Rep. 5 (2015) 17371.
[42] X. Dai, T. Chen, H. Cai, H. Wen, Y. Sun, ACS Appl. Mater. Interfaces 8 (23) (2016) 14572–14577.
[43] M. Wright, A. Uddin, Sol. Energy Mater. Sol. Cells 107 (2012) 87–111.

Zilei Wang is a M.S. candidate in Condensed Matter Physics in School of Physical Science and Technology at Lanzhou University. He received his B.S. degree in College of Physics and Information Engineering at Fuzhou University in 2015. His current research focuses on organic-inorganic hybrid solar cells.

Shanglong Peng received his B.S. degree (2003) in Physics and Ph.D. Degree (2008) in Condensed Matter Physics from Lanzhou University. He is currently a professor at School of Physical Science and Technology, Lanzhou University. His current research is focused on the design of Advanced Electronic and Energy Materials, and contort of surface and interface properties in energy related applications, mainly including solar cells and supercapacitor.

Yuxiang Wen received his B.S. degree in Physics from School of Physical Science and Technology at Lanzhou University in 2015. He is currently a postgraduate student in Condensed Matter Physics in School of Physical Science and Technology at Lanzhou University. His research interests focus on energy conversion and storage devices, including supercapacitors, lithium-ion batteries and solar cells.

Tianfeng Qin is currently a first-year Ph.D. student in the Key Laboratory for Magnetism and Magnetic Materials of the Ministry of Education, School of physical science and technology, Lanzhou University. He received his M.C. degree in Lanzhou University in 2017. His research interests mainly focus on the development of flexible and wearable all-solid-state energy storage and conversion device based on novel carbon materials and high-performance pseudocapacitor with high energy density.

Prof. Qiming Liu received his B.S. and M.S. degrees in Physics from Lanzhou University in 2008 and 2011, respectively. Then he had been awarded Japanese Government scholarship for his doctoral program in Saitama University, and in 2015, he achieved his Ph.D. degree of Engineering. Now he is a faculty member in Lanzhou University. His research focuses on the use of an integrated approach combining semiconductor physics, material, interface, device, and process engineering to improve the Photovoltaic Technology.

Dr. Deyan He received his B.S. degree (1982) and M.S. degree (1985) in Solid State Physics from Lanzhou University in China, and Ph.D. degree (1995) in Electronic Chemistry from Tokyo Institute of Technology in Japan. He is currently a professor at School of Physical Science & Technology, Lanzhou University. His current research involves development and application of Advanced Electronic and Energy Materials, mainly including silicon based thin films and metal oxides based materials for solar cells, Lithium ion batteries and other devices.

Guozhong Cao is Boeing-Steiner Professor of materials science and engineering, professor of chemical engineering, and adjunct professor of mechanical engineering at the University of Washington, and also a professor at Lanzhou University and Dalian University of Technology. His current research is focused on chemical processing of nanomaterials for energy related applications including solar cells, rechargeable batteries, supercapacitors, and hydrogen storage.